Rapid, One-Step, Digital Selective Growth of ZnO Nanowires on 3D Structures Using Laser Induced Hydrothermal Growth

*Junyeob Yeo, Sukjoon Hong, Manorotkul Wanit, Hyun Wook Kang, Daeho Lee, Costas P. Grigoropoulos, Hyung Jin Sung, and Seung Hwan Ko**

For functional nanowire based electronics fabrication, conventionally, combination of complex multiple steps, such as (1) chemical vapor deposition (CVD) growth of nanowire, (2) harvesting of nanowire, (3) manipulation and placement of individual nanowires, and (4) integration of nanowire to circuit are necessary. Each step is very time consuming, expensive, and environmentally unfriendly, and only a very low yield is achieved through the multiple steps. As an alternative to conventional complex multistep approach, original findings are presented on the first demonstration of rapid, one step, digital selective growth of nanowires directly on 3D micro/nanostructures by developing a novel approach; laser induced hydrothermal growth (LIHG) without any complex integration of series of multiple process steps such as using any conventional photolithography process or CVD. The LIHG process can grow nanowires by scanning a focused laser beam as a local heat source in a fully digital manner to grow nanowires on arbitrary patterns and even on the non-flat, 3D micro/nano structures in a safer liquid environment, as opposed to a gas environment. The LIHG process can greatly reduce the processing lead time and simplify the nanowire-based nanofabrication process by removing multiple steps for growth, harvest, manipulation/placement, and integration of the nanowires. LIHG process can grow nanowire directly on 3D micro/nano structures, which will be extremely challenging even for the conventional nanowire integration processes. LIHG does not need a vacuum environment to grow nanowires but can be performed in a solution environment which is safer and cheaper. LIHG can also be used for flexible substrates such as temperature-sensitive polymers due to the low processing temperature. Most of all, the LIHG process is a digital process that does not require conventional vacuum deposition or a photolithography mask.

1. Introduction

ZnO nanowires (NWs) is a very attractive material for optoelectronic devices because of its direct wide bandgap (3.27 eV) and large exciton binding energy (60 meV), and previous research has shown that ZnO NWs can be applied to various optoelectronics such as photovoltaic,[1] light-emitting devices (LEDs),[2] UV lasers,[3] and field emission devices.[4] Its piezoelectricity and n-type semiconducting behavior are also useful characteristics for the energy harvesting,[5] and electronics such as UV sensors[6] and field-effect transistors.[7]

Above all, one of great merits of ZnO NW is its ease of synthesis. While the conventional growth of metal-oxide nanowire using vapour-liquid-solid (VLS)[8] or vapour-solid (VS)[9] generally requires high temperature and vacuum environment, Greene et al.[10] reported facile hydrothermal growth of ZnO NW which can be conducted in a low temperature, non-vacuum and solution environment without the use of toxic chemicals and successfully acquired uniform ZnO NWs on a wafer scale. However, for more sophisticated device fabrication, local placement and integration of nanomaterials with other components are essential besides the nanomaterial growth. To take full advantage of ZnO NW synthesis

J. Yeo, S. Hong, M. Wanit, Prof. S. H. Ko
Applied Nano Tech and Science (ANTS) Lab
Department of Mechanical Engineering
KI for the Nano Century, KI for the optical science and technology
Korea Advanced Institute of Science and Technology (KAIST)
291 Daehak-ro, Yuseong-gu
Daejeon, 305-701, Korea
E-mail: maxko@kaist.ac.kr

H. W. Kang, Prof. H. J. Sung
Department of Mechanical Engineering
Korea Advanced Institute of Science and Technology (KAIST)
291 Daehak-ro
Yuseong-gu, Daejeon, 305-701, Korea

D. Lee, Prof. C. P. Grigoropoulos
Department of Mechanical Engineering
Laser Thermal Lab
University of California at Berkeley
Berkeley, CA 94720-1740, USA.

DOI: 10.1002/adfm.201203863

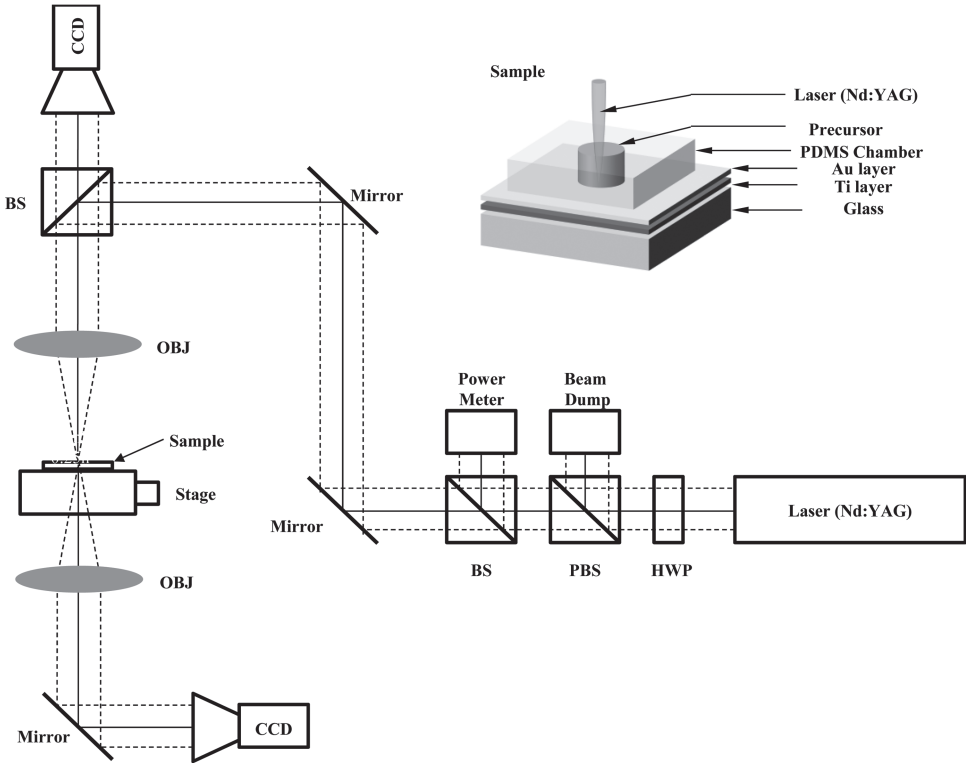

Figure 1. Dual inverted microscope set-up for laser induced hydrothermal growth (LIHG) of ZnO NWs. Focused Nd:YAG 532 nm laser was used as a local heat source.

simplicity, the associated nanomaterial patterning and integration steps, that are often necessary for device fabrication, have to be easy and compatible with such mild environment.

Numerous techniques, including dielectrophoresis,[11] microfluidics[12] and direct transfer[13] have been proposed to translate and align pre-synthesized ZnO NWs on specific places, but they require time consuming and expensive multi-steps for growth, harvesting and placement of nanowires even in a toxic and high temperature environment. Recently, instead of going through separate multiple steps for growth, harvesting and placement respectively, a series of new attempts of direct NW growth at specific places by combining growth, harvest and placement processing simultaneously have emerged. Patterning of a catalyst or a ZnO seed layer prior to the growth of NW has been conducted in order to grow ZnO NWs only at the selective area using conventional photolithography-based methods[14–16] and yielded uniform patterning of ZnO NWs. However, these methods involve several additional steps for exposure, develop and removal of the photoresist that increase the complexity of the process whereas the associated toxic chemicals also can damage certain substrates. Recently, new approaches for ZnO NW digital patterned direct growth have been introduced using microcontact printing[17] and inkjet printing.[18] These approaches succeeded in patterning ZnO NWs without the problem of the multi-step procedure, yet they still require a pre-made photo-mask or separate steps for the seed patterning and NW growth. Most of all, none of the above-mentioned NW local patterning processes could have possibly demonstrated non-flat, 3D microstructures. Therefore, there is a strong motivation to develop a single step, fully digital, maskless and high resolution ZnO NW local growth method even on the 3D microstructures.

In this study, we introduce a rapid and one-step selective digital direct growth of ZnO NWs by demonstrating a new method, called "laser induced hydrothermal growth" (LIHG) to achieve the growth and the patterning of NWs simultaneously and only at specific places without separate growth, harvest and placement steps. This method is low cost, low temperature, ambient pressure, and environmentally eco-friendly. By using laser as a local heat source, LIHG could grow the ZnO NW much faster than the conventional hydrothermal growth at a desired position without any mask or pre-patterned seed layer. Its resultant length is also measured to be considerably longer than the ZnO NW grown by conventional growth within a single pot without precursor solution refreshment. By manipulation of a tightly focused laser, arbitrary patterned ZnO NW growth could be achieved even on the 3D microstructures. This process is further applied to the fabrication of UV sensor by making a ZnO NW array network on the desired metal pattern on a glass substrate to confirm its applicability in device fabrication.

2. Results and Discussion

An overall schematic of the optics experimental setup is illustrated in **Figure 1**. Nd:YAG 532 nm continuous wave laser (Coherent, Millenna V) is focused by a long-working objective lens (OBJ1, Mitutoyo, 5X) at an arbitrary spot on the sample

where the typical intensity reaches up to several 10^4 W/cm^2. The reflected laser light is monitored by the same OBJ1 and appears at the upper CCD camera in conjunction with the sample surface image. In addition, a zoom lens with a notch filter for 532 nm is inserted between the CCD camera and objective lens in order to adjust the magnification of the vision and avoid the signal saturation of the CCD by scattered laser light, respectively. The laser power is then carefully controlled by the polarized beam splitter (PBS) and half wave plate (HWP). A power meter with a beam splitter (BS) is placed afterwards to measure the transmitted laser power in real-time. For in-situ observation of both front and back surfaces of the sample during the growth process, an additional objective lens (OBJ2) with a CCD module is located underneath the stage to constitute a dual inverted microscope system.

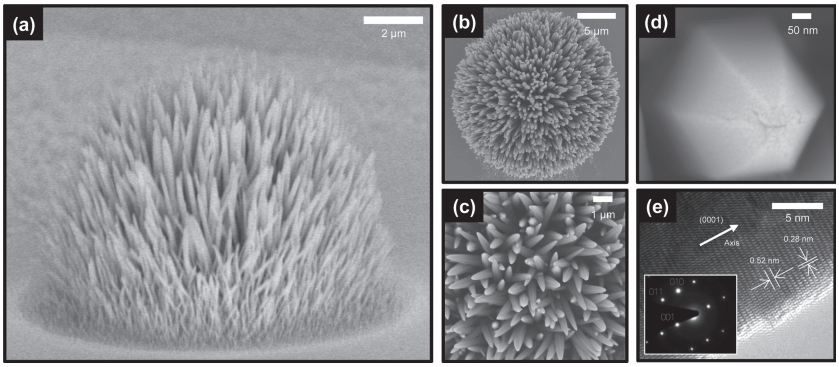

Figure 2. a) Tilted SEM picture of the ZnO NW array synthesized by LIHG. b) Top view SEM picture of the ZnO NW array. c) Magnified SEM picture of the ZnO NW array. d) Highly magnified SEM image of a single ZnO NW. e) High resolution TEM picture and SAED pattern of a single ZnO NW.

In conventional bulk growth (Supporting Information Figure S1), ZnO seeded substrate is immersed in a precursor solution at elevated temperature for a certain period of time[10] to grow ZnO NW uniformly on the substrate (Supporting Information Figure S2). The conventional ZnO NW hydrothermal growth is favorable at the elevated temperature (≈60–95°C) by bulk heating of precursor solution. Following the similar growth procedure (see the experimental section), an aqueous solution of 25 mM zinc nitrate hexahydrate ($Zn(NO_3)_2 \cdot 6H_2O$), 25 mM hexamethylenetetramine ($C_6H_{12}N_4$), and ≈5–7 mM polyethylenimine (C_2H_5N) is prepared as a precursor solution. The heating, reaction and NW growth by LIHG can be confined to a laser spot area by a focused laser. In our study, the laser is focused at an arbitrary position on the sample to photothermally raise the temperature and grow the NW only at the desired laser heated spot. The area subject to the temperature rise, or the resolution of the NW growth process, is closely related to the size of focused spot which can be easily reduced to several microns by tight focusing. LIHG has some common factors with the laser chemical vapor deposition (LCVD)[19] in that they both use a laser as a local heat source to locally induce the chemical reaction. However, the environment is totally different and LIHG is much more challenging in the liquid environment than LCVD in vacuum because the high probability for violent boiling and bubble generation in the liquid can destroy the NWs. At the cost of the challenging process, LIHG offers the significant advantage of using liquid environment, hence removing all complicated and expensive vacuum environment.

As the precursor solution does not absorb 532 nm wavelength laser light, the photothermal heating is mainly generated by laser absorption to the substrate. In order to provide a stable and uniform laser absorbing layer, titanium (Ti) and gold (Au) were sequentially deposited on a glass wafer using e-beam evaporator at the thicknesses of 30 nm and 220 nm, respectively.

For a typical experiment, several droplets of ZnO quantum dot (≈5–10 nm) seed solution (see the experimental section for synthesis) were deposited on a pre-cleaned substrate sample and rinsed with clean ethanol after several seconds to remove excess ZnO quantum dots. This coating step was repeated three times for the complete coverage of ZnO seed on the substrate. A small PDMS chamber was built on top of the sample and subsequently filled with the pre-made Zn precursor solution. The PDMS chamber filled with the Zn precursor solution was further enclosed with a cover glass to minimize the evaporation of the precursor solution and to maintain the flat top Zn precursor solution surface for good laser focusing and optical observation. The laser beam is then focused at the sample substrate to grow ZnO NWs where the entire growth process can be observed in-situ through CCD. A detailed configuration is schematically illustrated in the inset of Figure 1.

Figure 2 shows SEM and TEM pictures of ZnO NWs grown on the sample by LIHG for 20 min at 130 mW laser power. As shown in Figure 2a, the resultant ZnO NW assembly after complete growth resembles a hemispherical sea urchin shape as a whole. Such shape is due to the Gaussian laser beam profile at the surface. Although the temperature field of the precursor solution in the vicinity of the sample substrate surface generated by this Gaussian laser beam profile is not necessarily exactly Gaussian, it can be assumed to have analogous characteristics with the peak temperature at the center. In general, higher reaction temperature yields higher NW growth rate, hence longer NW. Therefore, the maximum temperature at the midpoint causes the NWs to grow longer with higher verticality compared to those at the edge due to the "crowding" effect originated from the competitive growth at the center. The NWs at the edge grow at a relatively slower rate and have more slanted angles resulting in an urchin-like semicircular ZnO NW array as shown in Figure 2a.

The beam waist radius of focused laser ($1/e^2$) is estimated to be ≈15 μm but the diameter of the ZnO NW array measured from its top view (Figure 2b) is bigger than the laser beam diameter due to the lateral thermal diffusion to the adjacent area, laser beam enlargement by scattering and the NW growth at the edge that extends outwards to the radial direction. It has been confirmed that the laser grown ZnO NWs can be as long as ≈10–12 μm with the diameter of ≈200–400 nm. The properties of the synthesized ZnO NW can be further controlled by various conditions including the magnification of the objective lens, the type of the substrate, the concentration of the

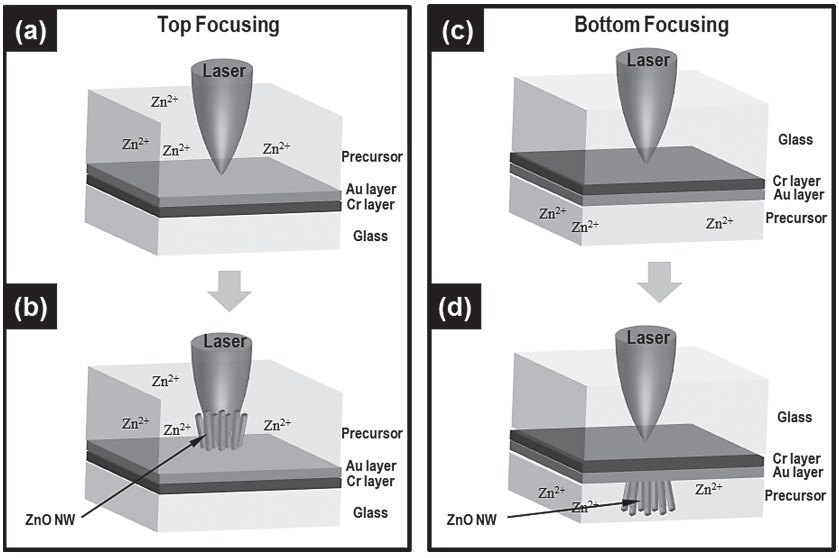

Figure 3. Schematic diagram of LIHG process by a,b) top focusing process and by c,d) bottom focusing. ZnO NWs grow on the same side of the substrate with the laser path for the top focusing and opposite side of the substrate for the bottom focusing.

precursor, the laser power and the growth time. The hexagonal cross-section and the diameter of ZnO NW can be verified from Figure 2c,d whereas the TEM image and the selected area electron diffraction (SAED) image (Figure 2e) confirm that the ZnO NW synthesized by LIHG are of single crystalline structure.

The laser beam irradiation configuration is important because the NW growth may disturb the laser irradiation and absorption to the substrate as the NWs get longer. The laser beam can be either (1) focused from the top ('top focusing' process, **Figure 3**a,b) on the same side of the substrate through the precursor solution or (2) from the bottom ('bottom focusing' process, Figure 3c,d on the opposite side of the substrate through the glass substrate. The illustrations in Figure 3 are exaggerated picture of the laser irradiation configuration (220-nm Au, 30-nm Ti layers on a 0.5-mm-thick glass substrate).

For the top focusing process (Figure 3a,b), ZnO NWs are synthesized on the same side with the laser beam path, hence the laser beam suffers from scattering by the grown NWs during the LIHG process. These optical disturbances reduce the laser power reaching the metal absorption layer to heat up the precursor solution, and thus maximum reaction temperature drops. On the other hand, for the bottom focusing process in Figure 3c,d, the NWs are growing on the opposite side of the laser irradiation, therefore NWs and laser beam have no direct interaction. The synthesized NWs no longer obstruct the laser beam path and the intensity profile at the absorbing layer remains unchanged throughout the synthesis process. Yet the temperature field induced by the laser is still time-dependent even for the bottom focusing process due to the interaction between the synthesized ZnO NWs and the medium. Having a slightly higher thermal conductivity (≈1 W/mK)[20] compared to the surrounding medium (water, 0.58 W/mK), ZnO NW can act as fins to dissipate the heat to the surrounding fluid as NWs grow longer. With the assumption that such dissipation of heat through the ZnO NW is the same in both cases, we can expect that the final NW length will be longer in the bottom focusing case at the same lasing condition. In addition to the longer NW and more stable growth condition, the bottom focusing is advantageous for real-time monitoring of the growth because the focusing and monitoring jobs are accomplished by two separate optical paths respectively.

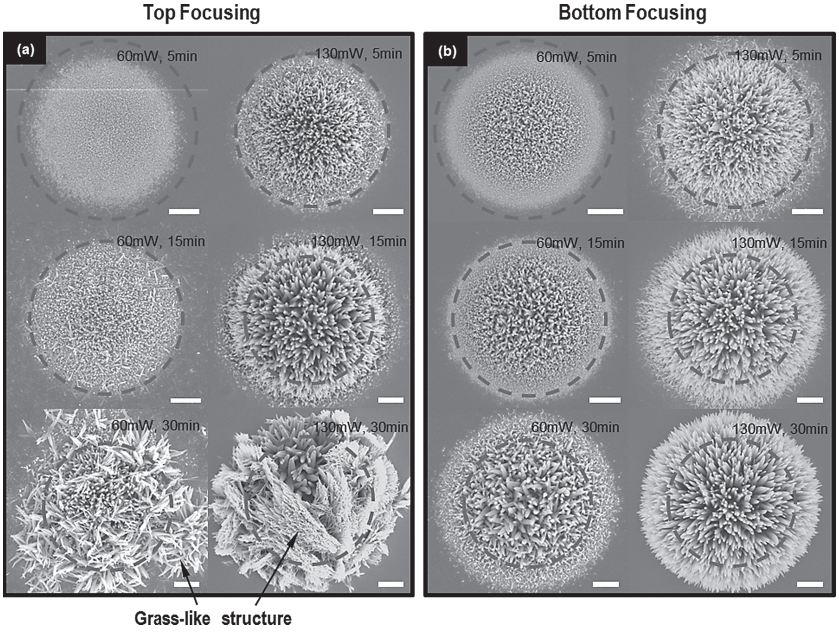

Figure 4. SEM pictures of ZnO NW array synthesized at various laser powers and laser irradiation times in top focusing process for a) top focusing and b) bottom focusing configuration. Dashed circles represent the size of laser spot with the diameter of 15 μm (scale bar: 3 μm). Pictures in left column and right column are outcomes at low power (60 mw) and high power (130 mW). Longer irradiation time makes the size of array larger with longer ZnO NW. In top focusing process, grass-like nanostructure are grown occasionally, at long irradiation time in particular, probably due to the change in the temperature field induced by the previously grown ZnO NWs. In bottom focusing process, ZnO NW array is grown better at higher power and longer irradiation time.

SEM images in **Figure 4** show ZnO NW arrays synthesized at different powers (60 and 130 mW) and illumination times (5, 15, and 30 min) by top (Figure 4a) and bottom focusing (Figure 4b). The laser spot size is designated by the dashed circles in Figure 4. The NW growth area is usually larger than the laser spot size for long laser irradiation because the precursor solutions at the edge

are subject to lower temperature and slower growth rate compared to those at the center and therefore they need longer laser irradiation time to be observable. Once the NWs start to grow at the edge of the NW growth area, they contribute to the increase in the NW array size because the horizontal ZnO NWs from the edge add extra lengths to the NW growth area.[18]

Higher power is desirable in this process as it increases the growth rate according to the Arrhenius relation, yet there exists an upper limit in the laser power because excessive laser power forms bubbles that destroy the synthesized ZnO NW array. We found that the optimum power should be around 130 mW to maximize the temperature without forming bubbles. The precision and uniformity of LIHG process was confirmed at this laser condition by fabricating 5×5 ZnO NW array on the planar sample as shown in Supporting Information Figure S3. It has been confirmed that the ZnO NW array growth could be completed within less than 30 min up to 10 μm length. Compared with the standard hydrothermal methods by bulk heating,[10,21–24] the ZnO NW grown by local laser heat source of LIHG method shows almost 10 times faster growth rate (20 μm/h) and ≈2–3 times larger length by a single pot process without precursor refreshment (Supporting Information Figure S4).

The much higher growth rate and longer length observed in the laser process compared with the conventional bulk heating hydrothermal method as shown in Supporting Information Figure S4 may be due to the steady supply of the Zn precursor via natural convection by temperature gradient and diffusion by concentration gradient (Supporting Information Figure S5, S6). In the conventional hydrothermal growth by bulk heating, the growth rate decreases asymptotically to zero with reaction time due to the total consumption of the Zn precursor in the solution and thus the precursor solution has to be replaced by fresh precursor repeatedly to extend the length further.[25] However, in LIHG process, the heated spot is limited only to the laser focus, and so is the consumption of Zn precursor. The precursor temperature outside the laser focal spot remains at room temperature and therefore its concentration mostly maintains at its original value to serve as a continuous Zn precursor supply source towards the laser growth spot. The temperature gradient generated by the laser heating also seems to be advantageous for the zinc precursor supply by creating a flow by the natural convection as shown in Supporting Information Figure S6.

It is worth mentioning that grass-like unexpected nanostructures are more occasionally found for the top focusing process, especially when the laser irradiation time is substantially long, as it is shown in two cases at the bottom of Figure 4a. For both cases, it is perceptible that the underlying structure is usual NWs, suggesting that the initial conditions were proper for the NW growth. However, as the temperature field changes quite randomly for longer reaction time during the growth for the top focusing process, previously grown ZnO NW array are sometimes covered by random shaped nano structures possibly due to the secondary nucleation caused by the instability and fluctuation in the temperature.

As the precursor solution and the glass substrate are both non-absorbing media, the stationary temperature field induced within the precursor solution and the glass substrate due to the heat transport from the laser heated surface in a spherical coordinate can be approximated by[26]

$$T^*(r^*) = \left[1 + (T_s^{m+1} - 1)\frac{1}{r^*}\right]^{1)(m+1)} \quad (1)$$

With $T* = T_s/T(\infty)$ and $r* = r/r_D$ where T_s, $T(\infty)$ and r_D correspond to the surface temperature, the ambient temperature and the radius of the reaction zone, respectively. The exponent m is related to the ambient material and the equation can describe the temperature distribution in liquid solution to a certain extent with a properly chosen exponent. However, once ZnO NW are grown on the Au thin film layer, the temperature field of the precursor induced by the laser is changed from its initial stage because the laser beam is disturbed by the grown NWs. To further investigate the initial temperature and the effect of the grown ZnO NW, COMSOL simulation (RF + heat transfer module) is conducted to calculate the electric field (TM mode) and the induced temperature field in the vicinity of the grown ZnO NW array numerically for both top and bottom focusing process. For simplicity, the structure has been approximated to 2D geometry where the length, angle and width of ZnO NW are arbitrarily chosen at a reasonable range that can reflect the actual ZnO NW structure grown by this process. The laser absorbing layer is assumed to absorb the incident laser perfectly converting the laser power into heat, and the temperature at the outermost boundary of the simulation space is fixed to be room temperature.

It can be confirmed from **Figure 5**a that the laser beam undergoes various optical disturbance for the top focusing process before it reaches the metal thin film layer on the substrate. Along the incident beam path, the laser is reflected from both absorbing layer and NW-precursor solution interfaces. Besides, large portion of laser power is lost to all radial directions due to the scattering. These disturbances result in a loss of the effective laser power reaching the laser absorbing surface and thus decrease the amount of photothermal heating lowering the temperature field induced by the top focusing process. On the contrary, for the bottom focusing process, laser power is fully absorbed by the laser absorbing layer as it is shown in Figure 5b. The temperature fields induced by the top and bottom focusing processes are illustrated in Figure 5c,d where it is evident that the temperature generated by the top focusing process is considerably lower (~85 °C) than that of the bottom focusing process (≈125 °C) at the same incident laser power. These values are comparable to the experimental estimation of the temperature at the laser focus using resistance temperature detector (RTD) method (Supporting Information Figure S7).

Another noticeable phenomenon is the laser guiding mode inside the NW which is due to the higher refractive index of ZnO (n = 2.03) compared to that of the ambient medium (n = 1.33). Such guiding modes can cause hot spots which are not favorable in terms of the reproducibility and stability of the process as the higher temperature is favorable for the bubble formation that can destroy the synthesized ZnO NWs. These complex optical interactions in the top focusing process are responsible for the different nanostructure aside from the NW as the temperature field changes randomly and sometimes meets the synthesis condition for unwanted nanostructure growth. This point is discussed further in Supporting Information Figure S8 by measuring the temperature evolution with time for both top and bottom focusing.

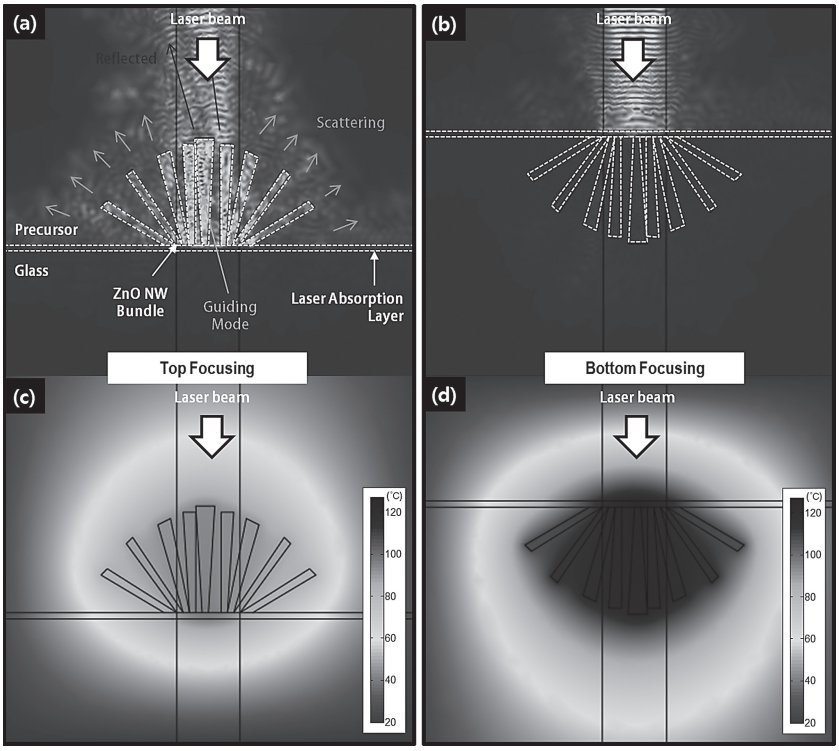

Figure 5. Laser energy (electric field) and interaction with nanowires simulation for a) top focusing and b) bottom focusing configuration for an arbitrary ZnO NW array calculated by Comsol software. The incident laser beam passes through previously grown ZnO NW array and undergoes several optical disturbances such as reflection and scattering for top focusing. For bottom focusing process, the incident beam remains unchanged by the growing ZnO NW. Resultant temperature field induced by c) top focusing and d) bottom focusing laser. The temperature field induced by bottom focusing process is relatively higher compared to that of top focusing process.

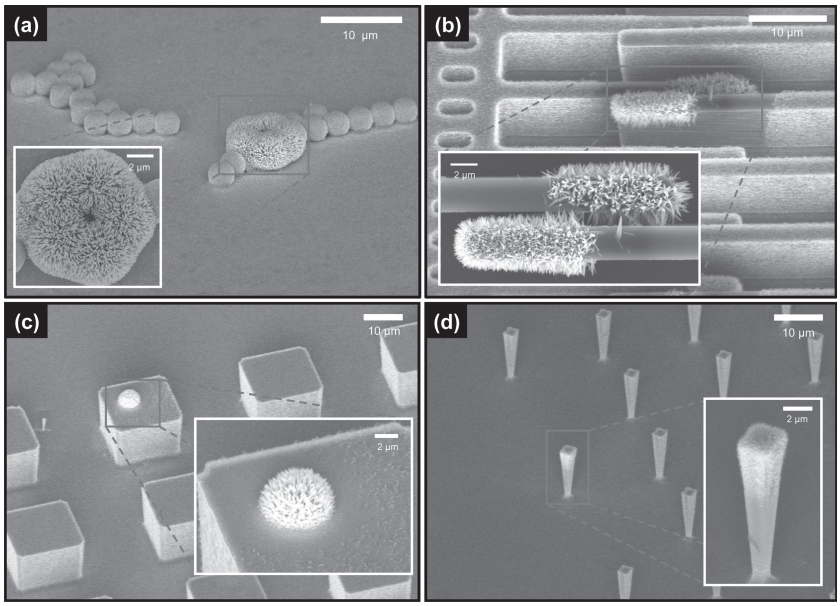

Figure 6. SEM pictures of the ZnO NW array on the various 3D micro structures. a) ZnO NW array is grown on the assembled silica beads. b–d) ZnO NW array grown on the Si microstructures on a Si wafer, which is etched by deep reactive ion etching (DRIE) after PR patterning. ZnO NWs are well grown on the arbitrary 3D micro structures. Inset picture is magnified SEM picture of the ZnO NW array in the box.

The NW integration on the non-planar microstructure is highly challenging even for the conventional method because it usually uses separate multi-steps for growth, harvesting and placement of NWs. Instead of applying time consuming, delicate multi-step processes, we develop a simple single step direct local NW growth at any places we want by combining the growth and placement simultaneously.

LIHG can be applied to local NW growth directly on the pre-made non-planar micro/nano-structures including arbitrary 3D structures. **Figure 6**a shows the ZnO NW array grown conformally on assembled silica microbeads (2-μm diameter, Microbeads, Bangslab). The boxed parts in Figure 6b–d show the ZnO NW array grown on the 3D microstructures fabricated on a silicon substrate using the conventional top-down photolithography with deep reactive ion etching (DRIE) process where a thin gold layer is deposited again as an absorbing layer. Usually the size of NW array is as big as the laser beam spot or slightly bigger. However, when the size of structure which the laser is irradiated on is smaller than the laser spot, the NW growth area is confined by the structure itself as shown in Figure 6b. In that figure, the microstructure is extended more than 20 μm in the horizontal direction while its width is confined to 3 μm. Accordingly, the growth area of the ZnO NW array is also confined to 3 μm in width, which is smaller than the irradiated laser beam spot. In addition, it is notable from the inset that two distinct microstructures can be connected by separated ZnO NW arrays when the distance between two microstructures is as small as the length of grown ZnO NWs. LIHG can be applied even for the sample with highly uneven profile in the vertical direction as illustrated in Figure 6c. The ZnO NW array is successfully synthesized on top of square-shaped island whose surface is located at 10 μm higher than the substrate simply by changing the laser focus position. ZnO NW can be further synthesized on area smaller than the laser spot located at an arbitrary vertical position as in Figure 6d. The tower-like structure in Figure 6d has a cross section as small as 2 μm × 2 μm while the height is extended to 10 μm in the vertical direction. The examples of ZnO NW grown on confined 1D lines and 2D islands also can be found in Supporting Information Figure S9 and S10. In brief, the ZnO NW array is directly grown on the microstructure of arbitrary size, height and shape in a single

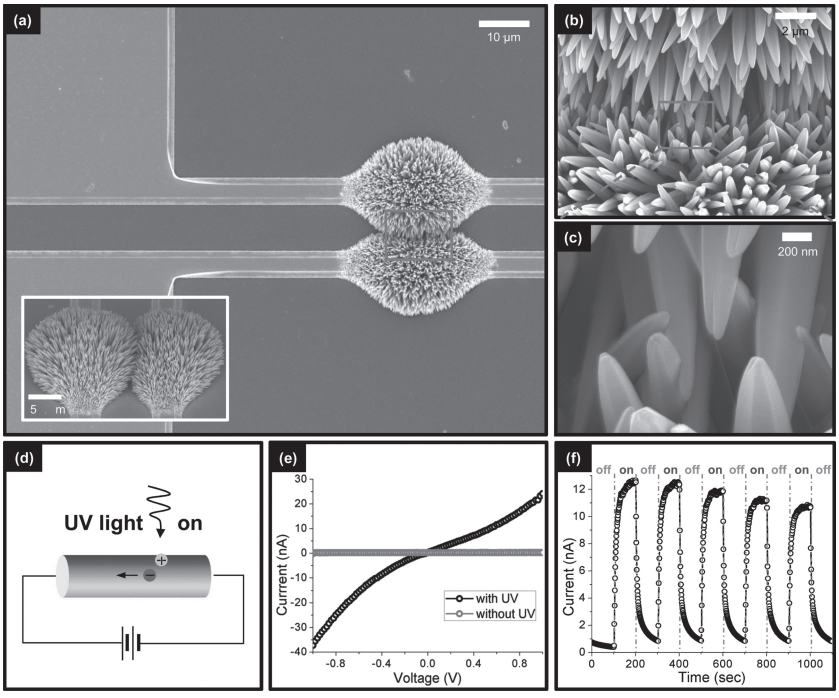

Figure 7. a) SEM pictures of the ZnO NW array network (NWAN). Inset picture is a tilted SEM picture of the ZnO NWAN. b) Magnified SEM picture of ZnO NW network area in the box in panel (a). c) Magnified SEM picture of contact region of the ZnO NW array in box in panel (b). Separately grown ZnO NW array makes a ZnO NW channel between two electrodes. d) Schematic diagram of photon-induced carrier transportation in a ZnO NW under UV illumination. e) *I–V* curves measurement of the ZnO network at room temperature with and without UV illumination. f) Photocurrent generation in the ZnO NWAN excited by a 365 nm UV lamp with 1 V external bias.

step by the LIHG process while the multisteps of NW harvest, manipulation, placement and integration on 3D microstructures should be applied separately in the conventional process, which will be extremely difficult.

ZnO, having a bandgap of 3.2eV, absorbs UV illumination to excite electrons in valence band to conduction band and generates an electron-hole pair. Among this photoinduced electron-hole pairs, a hole is trapped at the oxygen-related hole trapping states which generally exist at the surface of NW. Consequently, due to the unbalanced number of electron and hole, the recombination rate decreases and the carrier life time increases. The remaining electrons are either aggregated at the anode, readsorbed to the oxygen molecules at the surface or recombined with the ionized hole[27]. The reaction can be summarized as follows:

$$O_{2(g)} + e- \rightarrow O^-_{2(ad)} \quad (2)$$

$$hv \rightarrow e^- + h^+ \quad (3)$$

$$h^+ + O^-_{2(ad)} \rightarrow O_{2(g)} \quad (4)$$

Once the external bias is applied to ZnO NW, the remaining electron from Equation (3) is transported through the core of ZnO NW to increase the gain of photocurrent and thus the ZnO NW can be utilized as a UV sensor.

The ZnO NW array network (NWAN) fabricated for the UV sensor demonstration is depicted in **Figure 7** where two parallel gold electrodes are located 10 μm away from each other and connected by ZnO NW arrays. The LIHG process is applied to grow 10 μm ZnO NW array at the edge of each electrode pad. As the distance between two pads is shorter than the length of NW, two ZnO NW arrays can form a connected bridge network as shown in its cross sectional SEM picture in the inset of Figure 7a. Figure 7b is a higher magnification of the box area in Figure 7a. From Figure 7c we can confirm that individual NWs are contacted to form a ZnO NW channel between two pads. Figure 7d is a schematic diagram for measuring the performance of fabricated UV sensor. All measurements are conducted at ambient conditions where 365 nm wavelength UV lamp at 300 μW/cm^2 power (ENF-250C, Spectroline) is used for the UV illumination source. Typical current-voltage (*I–V*) characteristics of ZnO NWAN with and without UV illumination are shown in Figure 7e. In the measured *I–V* curve, the difference in conductance ranges up to almost ≈1–2 orders of magnitude. It is noticeable that the I-V curve shows asymmetry which is the phenomenon that has been previously reported elsewhere.[28,29]

The fabricated UV sensor basically consists of metal-semiconductor-metal (MSM) junction as the ZnO NW array (semiconductor) is grown on the Au (metal) pads. A schottky barrier is formed at each metal-semiconductor interface, yet two Schottky barriers are rather different as the inner part of ZnO NW is slightly inhomogeneous due to the intrinsic vacancies and defects that ZnO NW possess.[30] The difference between these two Schottky barriers contributes to the asymmetry of I-V curve or the generation of distinct photocurrent under UV illumination even without any biased voltage. [31]

Meanwhile, since the UV sensor fabricated by this process does not consist of a single ZnO NW but rather of a complex network formed by two distinct arrays of NWs, an infinitely small gap between two overlapping NWs has to be considered. According to previous studies, an additional tunneling effect has to be taken into account when an infinitely small gap is included to the modeling.[32] Therefore, we can expect that the measured I-V curve contains such tunneling effect as well.[33]

Figure 7(f) is the photocurrent measurement under repeated on-off states in accordance with the existence of UV illumination at room temperature with 1 V external bias. The current measured with the UV illumination is around 11 nA and this value is higher than the dark current which is normally under 1 nA.

3. Conclusions

We developed a new, direct digital local NW growth approach to pattern ZnO NW arrays directly on various samples. By using

focused laser as a localized heat source to induce controlled temperature rise, ZnO NW arrays have been successfully grown at an arbitrary position on a plane substrate, self assembled microbeads and 3D micro-structures, which will be almost impossible to achieve by the conventional multistep approach. The positioning precision and the area size of the growth are directly related to the laser spot size and it can be reduced down to several microns or even smaller, which is comparable to general photolithographic process. We also discovered that the growth rate of ZnO NW by laser local heating can be much faster and the length can be much longer than that of the conventional hydrothermal growth by bulk heating. Furthermore, its applicability to device fabrication has been confirmed by making ZnO NWAN for UV sensing.

By excluding the preparation of an absorbing layer, whole procedure for ZnO NW patterning is simplified to a great extent. The reduced number of procedure steps, together with higher growth rate, are expected to be beneficial for industrial use. Moreover, based on the hydrothermal growth, this process can be conducted in low temperature, non-vacuum and eco-friendly environment which are compatible for flexible plastic substrates as well.

4. Experimental Section

ZnO NPs Seed Synthesis: ZnO NPs seed synthesis is modified from Pacholski method.[34] 30 mM NaOH solution in ethanol is added slowly to 10 mM Zinc acetate dehydrate ($Zn(OAc)_2$, Sigma Aldrich) in ethanol and gently stirred for 2 h at 60 °C. The synthesized ZnO NPs are 5–10 nm in diameter with spherical shape and stable for at least two weeks in solution.

Precursor Solution Preparation for ZnO NW growth: An aqueous solution of 25 mM zinc nitrate hexahydrate ($Zn(NO_3)_2{\cdot}6H_2O$, Sigma Aldrich), 25 mM hexamethylenetetramine (HMTA, $C_6H_{12}N_4$, Sigma Aldrich), and ≈5–7 mM polyethylenimine (PEI, C_2H_5N, Sigma Aldrich) is heated at 95 °C for 1 h and cooled to room temperature and white precipitates were filter out.[10,25]

Electrical Characteristics Measurement for the UV Sensor: The fabricated ZnO NWAN for UV sensor is placed in probe station (MST5000A, MS Tech) with 4 axis micro manipulators having gold coated probe tips (10 μm in diameter) in a dark faraday cage. The current-voltage and photocurrent characteristics of UV sensor are measured using a semiconductor analyzer (HP4145B, Hewlett-Packard). The photocurrent is excited by a 365 nm wavelength UV lamp at 300 $\mu W/cm^2$ power (ENF-250C, Spectroline) on the UV sensor.

Supporting Information

Supporting Information is available from the Wiley Online Library or from the author.

Acknowledgements

J.Y and S.H. contributed equally to this work. This work is supported by National Research Foundation of Korea (NRF) (grant no. 2012-0008779, 2012-0003722), Global Frontier R&D Program on Center for Multiscale Energy System (grant no. 2012-054172), and the cooperative R&D Program (grant no. B551179-10-01-00) on the Korea Research Council Industrial Science and Technology and by EEWS-2012-N01120026 from KAIST EEWS Initiative.

Received: September 24, 2012
Revised: November 15, 2012
Published online: February 7, 2013

[1] M. Law, L. E. Greene, J. C. Johnson, R. Saykally, P. Yang, *Nat. Mater.* **2005**, *4*, 455.
[2] A. Nadarajah, R. C. Word, J. Meiss, R. Konenkamp, *Nano Lett.* **2008**, *8*, 534.
[3] M. H. Huang, S. Mao, H. Feick, H. Q. Yan, Y. Y. Wu, H. Kind, E. Weber, R. Russo, P. D. Yang, *Science* **2001**, *292*, 1897.
[4] D. Banerjee, S. H. Jo, Z. F. Ren, *Adv. Mater.* **2004**, *16*, 2028.
[5] S. Xu, Y. Qin, C. Xu, Y. Wei, R. Yang, Z. L. Wang, *Nat. Nanotechnol.* **2010**, *5*, 366.
[6] L. Luo, Y. Zhang, S. S. Mao, L. Lin, *Sens. Actuators, A* **2006**, *127*, 201.
[7] S. H. Ko, I. Park, H. Pan, N. Misra, M. S. Rogers, C. P. Grigoropoulos, A. P. Pisano, *Appl. Phys. Lett.* **2008**, *92*, 154102.
[8] R. S. Wagner, W. C. Ellis, *Appl. Phys. Lett.* **1964**, *4*, 89.
[9] K.-H. Lee, S.-W. Lee, R. R. Vanfleet, W. Sigmund, *Chem. Phys. Lett.* **2003**, *376*, 498.
[10] L. E. Greene, M. Law, J. Goldberger, F. Kim, J. C. Johnson, Y. Zhang, R. J. Saykally, P. Yang, *Angew. Chem., Int. Ed.* **2003**, *115*, 3139.
[11] J. Suehiro, N. Nakagawa, S.-i. Hidaka, M. Ueda, K. Imasaka, M. Higashihata, T. Okada, M. Hara, *Nanotechnology* **2006**, *17*, 2567.
[12] S. H. Lee, H. J. Lee, K. Ino, H. Shiku, T. Yao, T. Matsue, *J. Phys. Chem. C* **2009**, *113*, 19376.
[13] J. Kang, S. Myung, B. Kim, D. Oh, G. T. Kim, S. Hong, *Nanotechnology* **2008**, *19*, 095303.
[14] B. S. Kang, S. J. Pearton, F. Ren, *Appl Phys Lett.* **2007**, *90*, 083104.
[15] D. S. Kim, R. Ji, H. J. Fan, F. Bertram, R. Scholz, A. Dadgar, K. Nielsch, A. Krost, J. Christen, U. Gösele, M. Zacharias, *Small* **2007**, *3*, 76.
[16] Y.-J. Kim, C.-H. Lee, Y. J. Hong, G.-C. Yi, S. S. Kim, H. Cheong, *Appl. Phys. Lett.* **2006**, *89*, 163128.
[17] H. W. Kang, J. Yeo, J. O. Hwang, S. Hong, P. Lee, S. Y. Han, J. H. Lee, Y. S. Rho, S. O. Kim, S. H. Ko, H. J. Sung, *J. Phys. Chem. C.* **2011**, *115*, 11435.
[18] S. H. Ko, D. Lee, N. Hotz, J. Yeo, S. Hong, K. H. Nam, C. P. Grigoropoulos, *Langmuir* **2011**, *28*, 4787.
[19] Y. F. Guan, A. J. Pedraza, *Nanotechnology* **2008**, *19*, 045609.
[20] T. Olorunyolemi, A. Birnboim, Y. Carmel, O. C. Wilson, I. K. Lloyd, S. Smith, R. Campbell, *J. Am. Ceram. Soc.* **2002**, *85*, 1249.
[21] J. B. Baxter, A. M. Walker, K. v. Ommering, E. S. Aydil, *Nanotechnology* **2006**, *17*, S304.
[22] Y. I. Jeong, C. M. Shin, J. H. Heo, H. Ryu, W. J. Lee, J. H. Chang, C. S. Son, J. Yun, *Appl. Surf. Sci.* **2011**, *257*, 10358.
[23] J. Liu, X. Huang, Y. Li, X. Ji, Z. Li, X. He, F. Sun, *J. Phys. Chem. C* **2007**, *111*, 4990.
[24] S. Baruah, J. Dutta, *J. Cryst. Growth* **2009**, *311*, 2549.
[25] a) S. H. Ko, D. H. Lee, K. H. Nam, J. Y. Yeo, S. J. Hong, C. P. Grigoropoulos, H. J. Sung, *Nano Lett.* **2011**, *11*, 666; b) I. Herman, J. Yeo, S. Hong, D. Lee, K. H. Nam, J. Choi, W. Hong, D. Lee, C. P. Grigoropoulos, S. H. Ko, *Nanotechnology* **2012**, *23*, 194005.
[26] Dieter Bäuerle, *Laser Processing and Chemistry*, 4th ed., Springer, Berlin-Heidelberg, Germany **2011**, Ch. 9.
[27] C. Soci, A. Zhang, B. Xiang, S. A. Dayeh, D. P. R. Aplin, J. Park, X. Y. Bao, Y. H. Lo, D. Wang, *Nano Lett.* **2007**, *7*, 1003.
[28] O. Harnack, C. Pacholski, H. Weller, A. Yasuda, J. M. Wessels, *Nano Lett.* **2003**, *3*, 1097.
[29] C. S. Lao, J. Liu, P. Gao, L. Zhang, D. Davidovic, R. Tummala, Z. L. Wang, *Nano Lett.* **2006**, *6*, 263.
[30] H. Z. Zhang, X. C. Sun, R. M. Wang, D. P. Yu, *J. Cryst. Growth.* **2004**, *269*, 464.
[31] Z.-M. Liao, J. Xu, J.-M. Zhang, D.-P. Yu, *Appl. Phys. Lett.* **2008**, *93*, 023111.
[32] J. G. Simmons, *J. Appl. Phys.* **1964**, *35*, 2472.
[33] A. Menzel, K. Subannajui, F. Güder, D. Moser, O. Paul, M. Zacharias, *Adv. Funct. Mater.* **2011**, *21*, 4342.
[34] C. Pacholski, A. Kornowski, H. Weller, *Angew. Chem., Int. Ed.* **2002**, *41*, 1188.